Alaska Satellite Facility
ASF News & Notes
Summer 2005, volume 2:2

Examining Landfast Sea Ice on Alaska's Northern Coast

by Andy Mahoney, Hajo Eicken and Lew Shapiro, UAF Geophysical Institute; and Allison Graves, Nuna Technologies

Landfast sea ice is the largely stationary ice attached to the coasts of ice-covered seas. It is important to arctic coastal communities, which use it as an extension of the land for travel and to hunt marine mammals associated with the landfast ice and the adjacent system of leads.

Its presence reduces the effects of coastal erosion, and near-shore oil and gas development rely on landfast sea ice as a stable platform. Along the northern coast of Alaska, landfast sea ice is a seasonal phenomenon.

Beginning in late autumn, the landfast ice undergoes a gradual increase in area toward a stable extent before it experiences a rapid break-up and retreat in the following spring.

Punctuating this more gradual response to the unfurling of the seasons are episodic events, such as break-offs and stable extensions, which can have profound and lasting effects on the landfast ice and its denizens. Synthetic aperture radar provides imagery independent of weather and daylight with sufficient frequency to make it ideal for studying such events.

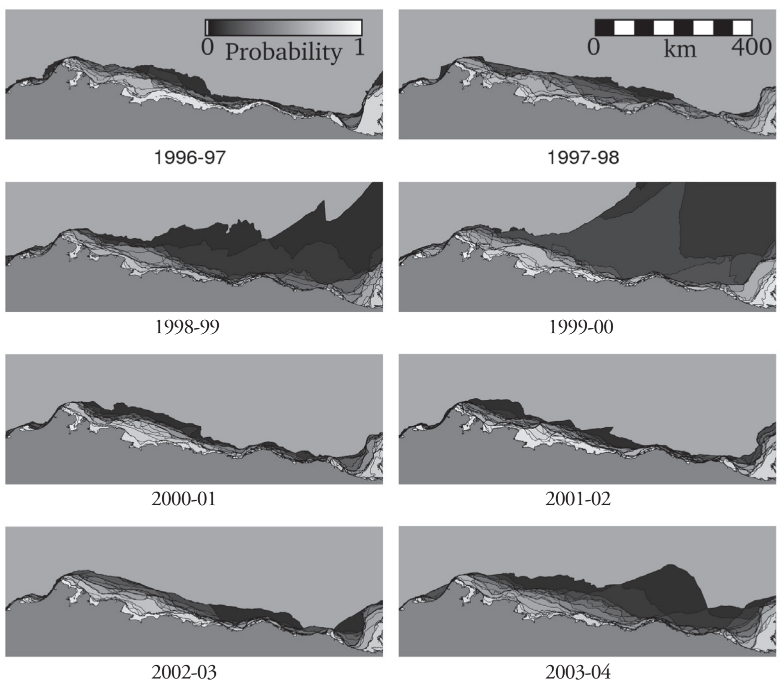

Probability of seasonal SLIE extent from 1996 — 2004.

More than 950 medium-resolution, calibrated GeoTIFFs of RADARSAT-1 ScanSAR data were used to generate collocated mosaics of the study area approximately every 10 days for the 8 ice seasons between 1996 and 2004. From the mosaics, we have delineated the seaward landfast ice edge (SLIE) 222 times. This has yeilded approximately 29 SLIEs per year between October and July as the landfast ice undergoes its annual cycle.

We apply a rigorous definition of landfast ice in this study, consisting of two criteria determined from remote sensing data: 1) that the ice is contiguous with the coast, and 2) that the ice lacks identifiable motion in three consecutive mosaics, or approximately 20 days.

Initial analysis revealed the asymmetric annual development of landfast ice, as defined above, with great inter-annual variability. Short-period episodic events such as stable extensions and a number of ice break-outs were also captured. The consequences of break-out events are of deep concern to those who use the landfast ice for travel, hunting or development.

Further, stable extensions of ice are found persisting for over a month up to 250km from shore in water over 200m deep. These extensions do not occur every year and the mechanisms responsible for their occurrence are not clear. However, the oceanographic and ecological implications of such a broad persistent barrier between the ocean and atmosphere warrant further investigation.

The data also revealed significant inter-annual variability in the maximum landfast ice extent according to our definition, but well inside this there is a zone in which the SLIE is more frequently located.

Within this zone the SLIEs converge at nodes where the variability throughout the year is less and the SLIE is more stable. These nodes lie along or close to the 20m isobath, which suggests they correspond to the locations of grounded ridges.

The figure to the left shows the landfast ice area associated with each SLIE stacked on top of each other to create maps indicating the number of occasions that landfast ice occupied any point in the study area for a given year. This can be viewed as the probability of finding landfast ice at any point between October and July. Each annual SLIE is shown in black, appearing as a probability contour. Stable nodes show up as regions of strong gradients in probability where SLIEs converge.

A comparison of our results with data compiled at the Geophysical Institute in the 1970s indicates that the SLIE has occupied a more shoreward position in recent years.

Further investigation is required to determine whether this reflects a change in the landfast ice regime or is a result of a different method of delineating landfast ice requires further investigation.

Upon completion of this project, all the derived products such as SLIE positions and mosaics will be publicly available.

Estimating Ice Thickness in Polynyas with Multiple Sensors

by Ben Holt, Jet Propulsion Laboratory, and Seelye Martin, University of Washington

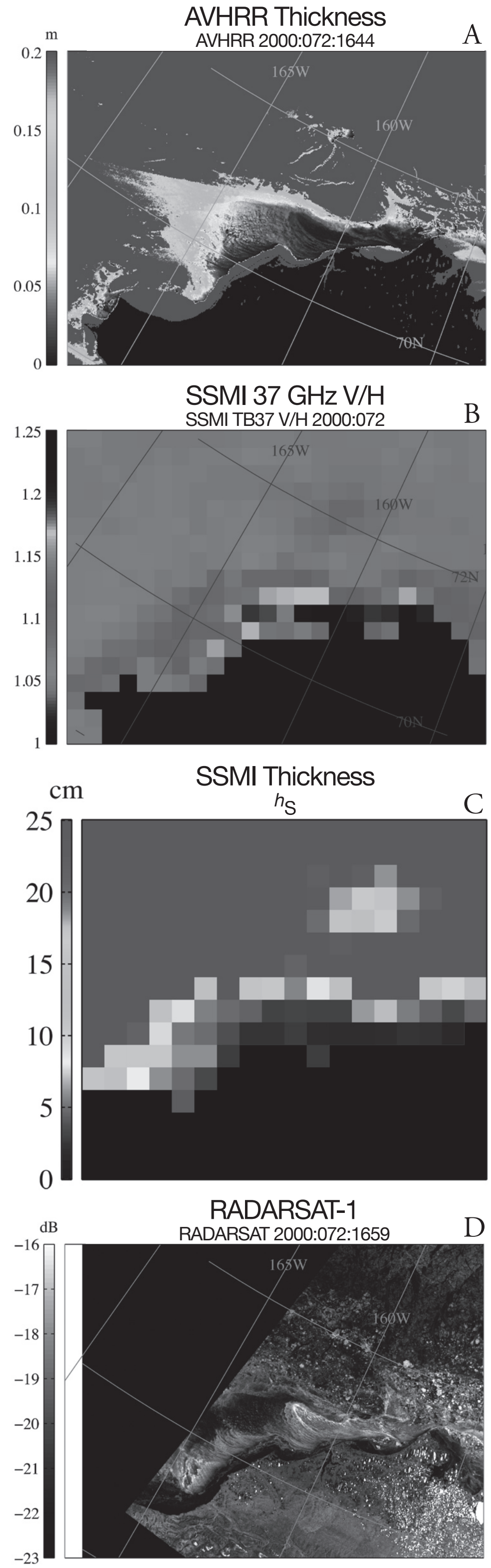

Each panel above contributes to a multisensor comparison of data taken on March 12, 2000 (day 72) over the extensive polynya found in the Chukchi Sea between Cape Lisbourne and Pt. Barrow, Alaska.

Polynyas are recurring regions of open water and thin ice within the polar sea ice cover, having intermittent openings and closings during winter. The large heat and salt fluxes related to the rapid ice formation and subsequent release of brine during polynya openings play key roles in coupling atmospheric heat loss with sea ice mass balance and oceanic circulation, particularly in the formation and maintenance of deep water layers in polar oceans.

We have applied an innovative algorithm to estimate thin ice thickness within arctic polynyas, using data from both the 37 GHz channel of the Special Sensor Microwave/Imager (SSM/I) and the 36GHz Advanced Microwave Scanning Radiometer-E (AMSR-E). The V/H polarization ratio of SSM/I data is sensitive to ice thickness from 0 to 10 cm, the thickness range with the largest heat flux from the ocean to the atmosphere. The algorithm enables daily observations using the extensive passive microwave time series and avoids discrepancies found in previous results that make use of ice concentration estimates.

Using same-day data taken over an extensive polynya found in the Chukchi Sea, a multisensor comparison is illustrated at the left. Panel A of the comparison reveals ice thicknesses up to 15 centimeters within the polynya region, based on the results from an ice-thickness algorithm using Advanced Very High Resolution Radiometer (AVHRR) data.

Panel B illustrates pixel-by-pixel values of the 25-km-resolution SSM/I data while panel C displays the resulting SSM/I ice thickness estimates. These two panels show, in turn, a good relationship to the AVHRR-derived thickness results at the top.

Data from the 36GHz AMSR-E sensor (not shown), with its 12.5km resolution, reveals even more detail than the SSM/I results, which further improves the estimate of polynya extent, especially closer to land where the largest heat flux occurs

Additionally, the RADARSAT-1 data in panel D provides an accurate and independent visual corroboration of the derived polynya extent.

Results from another study of the polynya, performed over 12 winters, demonstrate that the calculated heat losses are consistent with two years of temperature field data and overwinter salinity. The graph below shows how those results compare with numerical and satellite estimates of ice production. Although our results of ice production per unit area are smaller, the size of the 12-winter polynya study area was larger, so that our ice production estimates are of the same order.

The importance of our results is that the salt flux from the polynya is distributed over a much larger area than a model. This change in the salt distribution with distance from the coast will affect the offshore length scale of the oceanic response. We are currently extending our analysis to include the entire Arctic Ocean and the Ross Sea in Antarctica.

For more detailed information about the evolving development of this algorithm, see the following references:

Drucker, R., S. Martin, and R. Moritz (2003), Observations of ice thickness and frazil ice in the St. Lawrence Island polynya from satellite imagery, upward looking sonar, and salinity/temperature moorings, J. Geophys. Res., 108(C5), 3149, doi:10.1029/2001JC001213

Martin, S., R. Drucker, R. Kwok, and B. Holt (2004), Estimation of the thin ice thickness and heat flux for the Chukchi Sea Alaskan coast polynya from SSM/I data, 1990-2001, J. Geophys. Res., 109, C10012, doi:10.1029/2004JC002428

Martin, S., R. Drucker, R. Kwok, and B. Holt (2005), Improvements in the estimates of ice thickness and production in the Chukchi Sea polynyas derived from AMSR-E, Geophys. Res. Lett., 32, L05505, doi:10.1029/2004GL022013.

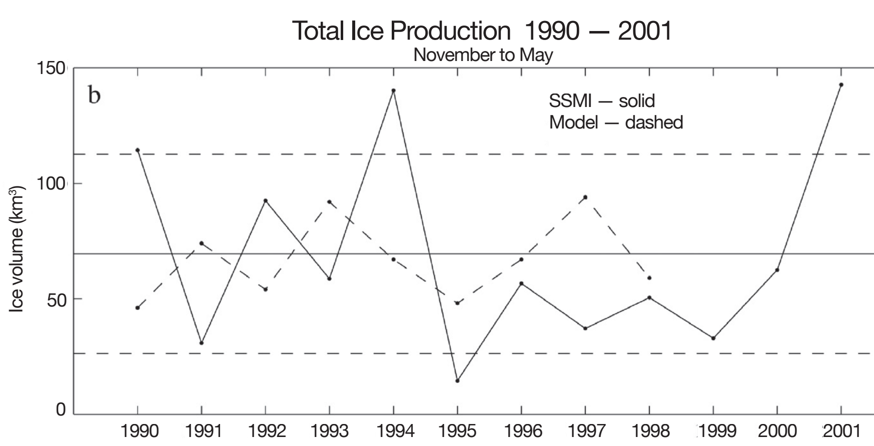

The graph at the right compares the results of two studies measuring annual Chukchi Sea polynya ice production. The solid line shows our SSM/I results while the dashed line gives the results from another polynya model of the same region.

Observing a Red Tide with Multiple Sensors

by John Ryan, Heidi Dierssen, Raphael Kudela, Christopher Scholin, Kenneth Johnson, James Sullivan, Andrew Fischer, Erich Rienecker, Patrick McEnaney, and Francisco Chavez; Monterey Bay Aquarium Research Institute

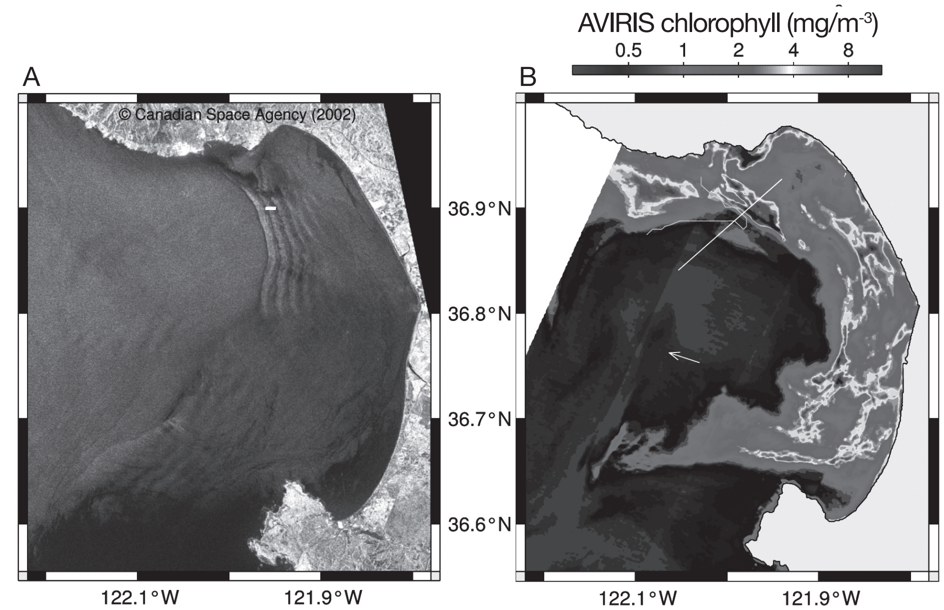

The images above exemplify the results of high-resolution, multidisciplinary remote sensing of a red tide and the biological-physical interactions that created bloom patchiness:
A) The Oct. 7 (02:04 GMT) RADARSAT-1 SAR image with a ~30m spatial resolution shows parallel dark-light bands pronounced in the northern bay, defining internal waves. The small, white scale bar across those wave fronts at 36.9°N is about 1km.
B) The Oct. 7 (21:01 GMT) AVIRIS image with a ~17m spatial resolution shows near-surface chlorophyll concentrations of the bloom represented in three shades: light gray at >3mg/m^{-3}, dark gray at >6mg/m^{-3}, and black at >12mg/m^{-3}.

Oceanic phytoplankton consists of many species, and dinoflagellates are among those phytoplankton species that cause reddish discoloration of surface waters when they bloom and accumulate near the surface. These conspicuous blooms, known as red tides, are of interest because they can have significant negative consequences for coastal marine life, fisheries and human health.

The adverse consequences of a red tide result primarily from introduction of toxins into the food web, direct physical harm to vital tissues (e.g., fish gills), and from oxygen depletion when the dense algae accumulations respire and decay. These impacts and the associated monitoring efforts can have significant economic consequences. Investigations of dinoflagellate ecology are central to understanding and predicting red tides. Such investigations are extremely challenging due to the complexity of rapidly changing coastal ocean environments and the rudimentary understanding of phytoplankton ecology.

Monterey Bay lies in the central California Current (CC) upwelling system where phytoplankton productivity and abundance are greatly augmented by wind-forced up-welling of deep, nutrient-rich waters to the shallow sunlit layer. During fall 2002, an intense and widespread red tide suddenly developed throughout the bay. The physical oceanography underlying this bloom was investigated using multidisciplinary observations from satellites, aircraft, ships and moorings.

Observed from the deck of a ship, the red tide was characterized by highly concentrated patches having sharp boundaries. Same-day high-resolution remote sensing from the Airborne Visible-Infrared Imaging Spectrometer (AVIRIS) and satellite SAR during the peak of the red tide detailed the extremely patchy nature of the bloom as well as processes that created the patchiness. We obtained some unique insights provided by this combination of high-resolution remote sensing at the height of the red tide.

Satellite ocean color and temperature imagery and observations from moorings described rapid and dramatic change when a filament of the CC swept through the bay. Observations from a ship-towed undulating vehicle, carrying a multidisciplinary instrument suite to monitor the bay also revealed extensive changes permeating the bay within a five-day period. Conditions became favorable for dinoflagellates, which led to red tide inception in the northern bay. Transport in coastal currents strongly influenced spread of the bloom throughout the bay and out into the adjacent sea.

Understanding patchiness of red tides is central to understanding their impacts, which are modulated by cell concentrations. One process creating patchy aggregations of dinoflagellates is the interaction of swimming with convergent circulation. They move in vertical migrations that enable access to the resources they need to grow: light that increases in intensity toward the surface, and nutrients that increase in concentration with depth.

They may also use motility to stay near the surface in the presence of downward vertical currents. Where horizontal currents converge and create downward flow, dinoflagellates will be concentrated near the surface if they can swim upward at a rate greater than that of the downward currents.

Internal waves (IW), which vertically displace and propagate along subsurface density layers, are a ubiquitous physical forcing in coastal ocean environments, and they create convergence zones oriented parallel to and overlying the waves. IW are evident in SAR imagery because they modify ocean surface roughness in bands along the wave fronts. The SAR image on this page revealed an IW packet in northern bay waters. The white, 1km scale bar at 36.9°N defines an IW wavelength of ~1km. The same scale was evident in the wavelike spatial pattern of a red tide patch in this region, supporting the influence of IW on red tide patchiness.

An earlier SAR image (not presented here) showed no evidence of IW in the region of this patch, thus it is possible that the dinoflagellate aggregations retained an imprint of IW influence from the wave packet shown in the figure. Combining these high-resolution measurements with coarser resolution satellite sea surface temperature and mooring observations showed that at larger scales than the IWs, convergence created by the confluence of water masses also influenced bloom patchiness.

Multiple physical phenomena occurring across a wide range of scales forced initiation and development of this red tide in Monterey Bay. Such biological-physical interactions can only be discerned through multidisciplinary, multi-scale sensing. In situ observations from moorings, ships and autonomous underwater vehicles in the bay provided a rich interpretive framework upon which to build with advancing capabilities in remote sensing.

Meeting Calendar

Arctic Science Conference (AAAS), September 27-29, Kodiak, AK, United States
http://arctic.aaas.org/meetings/

Geological Society of America, October 16-19, Salt Lake City, UT, United States
http://www.geosociety.org/meetings/

Sixth Fire and Forest Meteorology Symposium, October 25-27, Canmore, AB, Canada
http://www.ametsoc.org/meet/fainst/fireandforest.html

International Arctic Sea Ice Thickness Workshop, November 8-9, Copenhagen, Denmark
http://www.iasc.no/ (link, "Side meetings around ICARP II")

Second International Conference on Arctic Research Planning (ICARP II), November 10-12, Copenhagen, Denmark
http://www.iasc.no/

Fall American Geophysical Union Meeting, December 5-9, San Francisco, CA, United States
http://www.agu.org/meetings/fm05/

International Glaciological Society Symposium on Sea Ice, December 5-9, Dunedin, New Zealand
http://www.igsoc.org/symposia/2005/dunedin/

Submissions and Subscriptions

This newsletter, published by ASF, was created to provide detailed information about special projects and noteworthy developments, as well as science articles highlighting the use of ASF data.

To receive the newsletter by postal mail, please fill out the subscription form linked to the ASF homepage at www.asf.alaska.edu. Current and back issues of the newsletter can be obtained in PDF format through the ASF Web site.

Submissions to the News & Notes and suggestions about content are always welcome. If you are interested in contributing materials, please call or send an email to the editor:

Cheryl Katje, ASF User Services
907-474-6166
uso@asf.alaska.edu.

Alaska Satellite Facility
UAF Geophysical Institute
903 Koyukuk Drive
PO Box 757320
Fairbanks, AK 99775-7320

www.asf.alaska.edu